




**Kernel function based quantum algorithms for finite temperature quantum simulation**Hai Wang <sup>1,2,\*</sup> Jue Nan,<sup>1,2,\*</sup> Tao Zhang,<sup>3</sup> Xingze Qiu <sup>1,2</sup> Wenlan Chen <sup>3,4,†</sup> and Xiaopeng Li<sup>1,2,5,‡</sup><sup>1</sup>*State Key Laboratory of Surface Physics, Institute of Nanoelectronics and Quantum Computing, and Department of Physics, Fudan University, Shanghai 200438, China*<sup>2</sup>*Shanghai Qi Zhi Institute, Shanghai 200030, China*<sup>3</sup>*Department of Physics and State Key Laboratory of Low Dimensional Quantum Physics, Tsinghua University, Beijing 100084, China*<sup>4</sup>*Frontier Science Center for Quantum Information, Beijing 100084, China*<sup>5</sup>*Shanghai Research Center for Quantum Sciences, Shanghai 201315, China*

(Received 5 February 2022; revised 20 August 2022; accepted 20 June 2023; published 1 August 2023)

Computing finite temperature properties of a quantum many-body system is key to describing a broad range of correlated quantum many-body physics from quantum chemistry and condensed matter to thermal quantum field theories. Quantum computing, which has seen rapid developments in recent years, has a huge potential to impact the computation of quantum thermodynamics. To fulfill these potential impacts, it is crucial to design quantum algorithms that utilize the computation power of quantum computing devices. Here, we present a quantum kernel function expansion (QKFE) algorithm for solving thermodynamic properties of quantum many-body systems. In this quantum algorithm, the many-body density of states is approximated by a kernel Fourier expansion, whose expansion moments are obtained by random state sampling and quantum interferometric measurements. Compared to its classical counterpart, namely, the kernel polynomial method (KPM), QKFE has an exponential advantage in the cost of both time and memory. In computing low temperature properties, QKFE becomes inefficient, similar to classical KPM. To resolve this difficulty, we further construct a thermal ensemble iteration (THEI) protocol which starts from the trivial limit of an infinite temperature ensemble and approaches the low temperature regime step by step. For quantum Hamiltonians, whose ground states are preparable with polynomial quantum circuits, THEI has an overall polynomial complexity. We demonstrate its efficiency with applications to one- and two-dimensional quantum spin models and a fermionic lattice. With our analysis of the realization with digital and analog quantum devices, we believe the quantum algorithm is accessible to current quantum technology.

DOI: [10.1103/PhysRevB.108.085102](https://doi.org/10.1103/PhysRevB.108.085102)**I. INTRODUCTION**

The computation of thermodynamic quantities of quantum Hamiltonians is at the core of simulating correlated electrons in quantum materials and complex molecules [1,2]. The exponential complexity in treating a large number of entangled degrees of freedom on a classical computer prevents accurate determination of macroscopic physics [3,4], causing a generic challenge to our quantitative description of a broad range of strongly correlated quantum phases, from quantum magnetism [5] and high  $T_c$  superconductivity [6] to neutron star matters [7].

With controllable quantum systems, one method that has been carried out is to synthesize analog Hamiltonian models and extract thermodynamic properties by preparing experimental systems at thermal equilibrium [8–10]. Strongly correlated physics, such as the Mott-superfluid transition [11,12], unitary Fermi gas [13], and antiferromagnetism [14–16], has been accomplished with cold atoms. With

rapid advancement of programmable quantum devices in the last several years, such as superconducting qubits [17–20], trapped ions [21,22], entangled photons [23–27], and Rydberg atoms [28–31], research interest in developing algorithmic approaches for quantum simulations has been growing [32–37]. Much progress has been made in relation to determining ground states considering variants of quantum phase estimation [38,39], adiabatic Hamiltonian evolution [40,41], and variational quantum circuits [1,2,42,43]. Quantum algorithms for finite temperature quantum simulations have also been proposed using generalized Metropolis sampling [32,36,44,45], quantum Lanczos methods [34], and variational thermofield double-state algorithms [46–48]. However, until now, finite temperature quantum simulation algorithms have been relatively scarce compared to ground state computations. Efficient computation methods for free energy and thermal entropy, which are crucial for determining thermodynamics, are particularly lacking and in great demand.

In this work, we introduce a quantum kernel function expansion (QKFE) algorithm in which the energy dependence of observables and many-body density of states (DOS) are represented by Fourier series. We show that the expansion moments can be measured by quantum circuits with polynomial cost, achieving an exponential quantum advantage over

\*These authors contributed equally to this work.

†cwlaser@ultracold.cn

‡xiaopeng\_li@fudan.edu.cn

the classical analog, namely, the kernel polynomial method (KPM) [49]. The QKFE quantum circuit is fully deterministic, i.e., free of variational optimization, in sharp contrast to variational quantum algorithms [46–48] and quantum Lanczos methods [34,50–52]. The infamous barren plateau problem [53,54] is thus completely absent with QKFE. The overall complexity of QKFE is exponential in approaching the low temperature properties of a generic Hamiltonian. This is a corollary of Hamiltonian QMA completeness, a complexity class of languages that can be probabilistically verified by a quantum verifier in polynomial time [55–57]. We further develop a thermal ensemble iteration protocol based on QKFE with Hamiltonian evolutions which computes thermodynamic quantities such as local observables, free energy, and thermal entropy with polynomial complexity, provided that the ground state of the Hamiltonian can be prepared at a polynomial cost.

## II. QUANTUM KERNEL FUNCTION EXPANSION

Our QKFE algorithm is inspired by the classical KPM. Considering a many-body system with Hamiltonian  $\hat{H}$ , a physical quantity that is natural for the KPM to compute is the DOS [49], which is defined as  $\rho(E) = \frac{1}{D} \sum_i \delta(E - E_i)$ , with  $E_i$  being the eigenvalues and  $D$  being the Hilbert space dimension. For convenience in theoretical treatment, the energy spectra are assumed to be bounded between  $E_{\min}$  and  $E_{\max}$ . A dimensionless energy

$$\epsilon \equiv (E - E_{\min})/(E_w + 0^+) \in (0, 1) \quad (1)$$

is introduced accordingly, with  $E_w$  being  $E_{\max} - E_{\min}$ . We then have a rescaled Hamiltonian,  $\hat{\mathcal{H}} = (\hat{H} - E_{\min} \mathbb{1})/(E_w + 0^+)$ . This rescaling can always be performed for a lattice Hamiltonian with a finite Hilbert space dimension. In the classical KPM, the DOS is expanded in terms of the Chebyshev polynomial  $T_n(\epsilon)$ , that is,

$$\rho(\epsilon) = \left[ \mu_0 + 2 \sum_{n=1}^N \mu_n T_n(\epsilon) \right] / (\pi \sqrt{1 - \epsilon^2}).$$

The expansion moment  $\mu_n = \text{Tr}[T_n(\hat{\mathcal{H}})]$  can be evaluated stochastically via a small number  $R$  of random states  $|r_0\rangle$ :

$$\mu_n \approx \frac{1}{R} \sum_{r=1}^R \langle r_0 | r_n \rangle,$$

where  $|r_n\rangle = T_n(\hat{\mathcal{H}})|r_0\rangle$  is determined by the recursion relation  $|r_n\rangle = 2\hat{\mathcal{H}}|r_{n-1}\rangle - |r_{n-2}\rangle$ . This approach has been used in classical computing for finite energy properties of large matrices and has led to great success in solving noninteracting Anderson localization problems [49]. Nonetheless, the Hamiltonian multiplication has a cost linear to the Hilbert space dimension  $D = 2^L$  for a system of  $L$  qubits. Therefore, the required time and memory both scale exponentially with the number of spins, which has limited its application in simulating more complex quantum many-body systems.

In this section, we present an efficient quantum algorithm for computing the expansion moments that has an exponential quantum speedup over the classical KPM.

### A. QKFE algorithm

Instead of Chebyshev polynomial expansion as used in the classical KPM, in our QKFE algorithm we perform a Fourier expansion for the DOS,

$$\rho(\epsilon) = c_0 + 2 \sum_{n=1}^{N-1} c_n \cos(n\pi\epsilon), \quad (2)$$

because the Fourier moments are more convenient to use quantum computing than the Chebyshev polynomial expansion. We introduced a large-moment cutoff  $N$  for the expansion. By writing the Fourier moments in the form of

$$c_n = \frac{1}{D} \text{Re}\{\text{Tr}[e^{-in\pi\hat{\mathcal{H}}}]\}, \quad (3)$$

we find these moments can be obtained efficiently with a quantum circuit, as shown in Fig. 1(a), which contains  $L$  physical qubits and one ancilla qubit. The step of averaging  $\text{Tr}[\dots]/D$  is performed by sampling Haar random states, whose computation efficiency relies on quantum typicality [59–61]. Despite the difficulty in preparing exact Haar randomness, it can be approximated by relatively shallow circuits [58,62–65]. It has been shown that the required circuit depth to converge to unitary- $t$  designs scales polynomially with the number of qubits [53].

The procedure for measuring  $c_n$  involves three steps. The first step is to choose  $R$  random product states as the circuit input and scramble these states by performing local random unitary operations  $\hat{U}_s$ , following the strategy in Ref. [58]. Here,  $\hat{U}_s$  consists of individual cycles, with each cycle composed of local one- and two-qubit gates, following the strategy in Ref. [58]. The second step is to apply a control unitary operation,

$$|0\rangle\langle 0| \otimes I + |1\rangle\langle 1| \otimes e^{-in\pi\hat{\mathcal{H}}}, \quad (4)$$

across the ancilla qubit and the system. We then take measurements. The measurement outcomes of  $\hat{\sigma}_x$  on the ancilla qubit average to the  $c_n$  moment. Since the results of quantum measurement following the quantum circuit are directly related to the Fourier moments, instead of to the trace, estimating the Fourier moments does not require exponential precision of the quantum measurement (for more details see Sec. II C).

In addition to the DOS, the energy dependence of the local observables can be obtained efficiently using the same quantum circuit [Fig. 1(a)]. We consider a general local observable  $\hat{A}$ , which, for example, could represent spin polarization or correlation functions. Its energy dependence is given by  $\alpha(\epsilon) = \langle \epsilon | \hat{A} | \epsilon \rangle$ , with  $|\epsilon\rangle$  being an eigenstate of  $\hat{\mathcal{H}}$  with energy  $\epsilon$ . The Fourier expansion reads

$$\alpha(\epsilon)\rho(\epsilon) = d_0 + 2 \sum_{n=1}^{N-1} d_n \cos(n\pi\epsilon), \quad (5)$$

with the moments

$$d_n = \frac{1}{D} \text{Re}\{\text{Tr}[\hat{A} e^{-in\pi\hat{\mathcal{H}}}]\}. \quad (6)$$

This implies the  $d_n$  moments can be measured by the same quantum circuit as  $c_n$ . The measurement outcome of the tensor

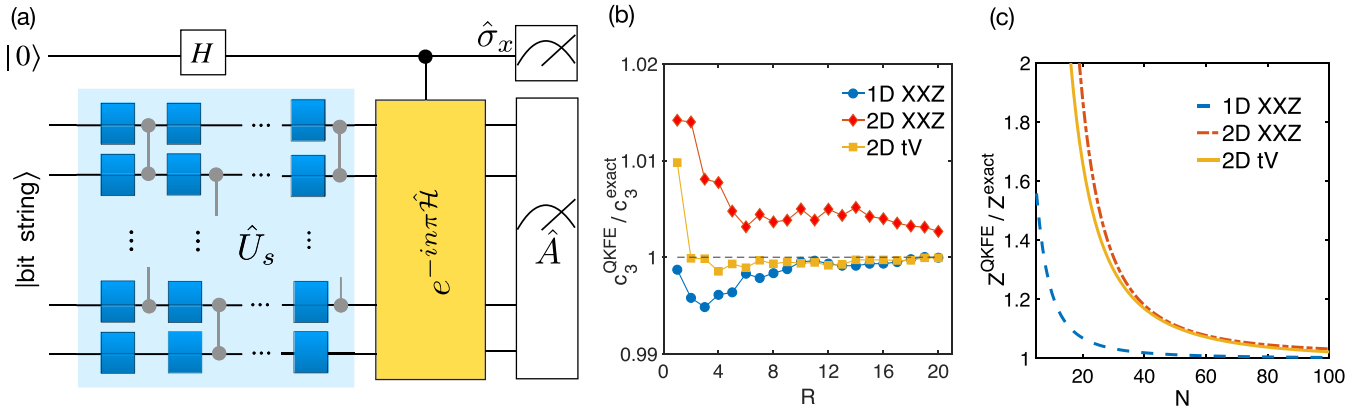


FIG. 1. The quantum kernel function expansion algorithm. (a) An illustration of quantum circuits for measuring Fourier expansion moments. The random circuits in blue are constructed following Ref. [58] using 40 cycles, with each cycle consisting of one layer of random single-qubit gates and one layer of CZ gates. (b) The convergence of one typical expansion moment,  $c_3$ , with an increasing number of random states  $R$ . (c) The convergence of the partition function with an increasing expansion cutoff  $N$ . The blue, red, and orange lines correspond to the results of the 1D-XXZ [Eq. (14)], 2D-XXZ [Eq. (15)], and  $t$ -V [Eq. (16)] models, respectively. In (b) and (c), the QKFE results of the expansion moment  $c_3$  and the partition function  $Z$  ( $c_3^{\text{QKFE}}$  and  $Z^{\text{QKFE}}$ ) are normalized by their exact values. Here, we choose  $L = 18$  for the 1D model and a square lattice with  $4 \times 4$  geometry for the 2D models. The temperature is fixed at  $T = 3$ .

product of  $\hat{\sigma}_x$  (ancilla) and  $\hat{A}$  (local observables) in the final state of the quantum circuit averages to the  $d_n$  moments.

Having the Fourier moments  $c_n$  and  $d_n$  computed by the quantum circuit, we reconstruct the functions  $\rho(\epsilon)$  and  $\alpha(\epsilon)$ . With the energy dependence of the DOS and local observables computed, the partition function  $Z(\beta) = \text{Tr}[e^{-\beta\hat{H}}]$  as a function of the inverse temperature  $\beta$  and the canonical ensemble average  $A(\beta) = \text{Tr}[\hat{A}e^{-\beta\hat{H}}]/Z(\beta)$  are then given by

$$Z(\beta) = \int_0^1 e^{-\beta E_w \epsilon} \rho(\epsilon) d\epsilon, \quad (7)$$

$$A(\beta) = \frac{1}{Z(\beta)} \int_0^1 e^{-\beta E_w \epsilon} \alpha(\epsilon) \rho(\epsilon) d\epsilon. \quad (8)$$

With the partition function, all thermodynamic quantities such as free energy and thermal entropy can then be obtained [66].

In the physical implementation of our QKFE algorithm, the quantum circuit in Fig. 1(a) can be further decomposed into local quantum gates by considering Trotterization, for which the circuit depth for extracting the Fourier moments  $c_n$  and  $d_n$  scales as  $\mathcal{O}(n\delta_t^{-1})$ , with  $\delta_t$  being the Trotterization step. One specific example is provided in Sec. IV A. In comparison with the classical analog, namely, the classical KPM, our QKFE algorithm has an exponential speedup in computing the expansion moments—the time cost for the classical KPM is exponential, whereas it is polynomial in QKFE. We emphasize here that the QKFE algorithm is free of variational optimization as its quantum circuit is fully deterministic. This makes the QKFE algorithm rather unique in comparison with variational quantum algorithms [46,47] and quantum Lanczos methods [34,50–52], for which the variational optimization could be costly in practical computation and sometimes encounters the infamous barren plateau problem [53,54]. Since the QKFE algorithm involves a block of control unitaries as in deterministic quantum computation with one clean qubit (DQC1), whose quantum advantage has been established [67,68], it is worth extending the computation complexity

analysis for DQC1 to QKFE, which we expect to provide a computation theoretic foundation for the quantum advantage for QKFE. This is left for future investigation.

### B. Uniform convergence by kernel function expansion

In reconstructing the functions  $\rho(\epsilon)$  and  $\alpha(\epsilon)$ , we need to correct the moments by multiplying the Jackson kernel in order to damp out the cutoff-induced Gibbs oscillations. It is well known that to approximate an analytic function  $F(\epsilon)$ , the  $N$ th-order Fourier series expansion  $F_N(\epsilon) = c_0 + 2 \sum_{n=1}^{N-1} c_n \cos(n\pi\epsilon)$  has a norm convergence. However, uniform convergence is required here for computing the energy dependence of the local observables and the DOS. We apply kernel functions to the Fourier expansion. For a continuous function  $f(x)$  with  $x \in (-1, 1)$ , it has been shown in classical KPM analysis [49] that the kernel function corrected  $N$ th-order Chebyshev expansion  $f_N(x) = \tilde{c}_0 + 2 \sum_{n=1}^{N-1} \tilde{c}_n T_n(x)$  has a uniform convergence to  $f(x)$ , with

$$\tilde{c}_n = h_n \int_{-1}^1 \frac{f(x) T_n(x)}{\pi \sqrt{1-x^2}} dx,$$

$$h_n = \frac{1}{N+1} \left[ (N-n+1) \cos \frac{\pi n}{N+1} + \sin \frac{\pi n}{N+1} \cot \frac{\pi}{N+1} \right],$$

$$T_n = \cos[n \arccos(x)],$$

where  $h_n$  is the Jackson kernel [69]. Approximating  $f(x)$  by  $f_N(x)$  has an error [49]  $\|f(x) - f_N(x)\|_\infty \sim w_f(1/N)$ , with  $w_f(\delta) = \max |f(x) - f(y)|_{|x-y| \leq \delta}$ . This can be interpreted as an error on the order of  $\mathcal{O}(1/N)$ .

The Fourier expansion used in our work is related to the Chebyshev expansion by taking  $x = \cos(\pi\epsilon)$ , and  $F(\epsilon) = f(\cos(\pi\epsilon))$ . For  $\epsilon \in (0, 1)$ , we have  $T_n(x) = \cos(n\pi\epsilon)$ . It follows immediately that

$$\|F(\epsilon) - F_N(\epsilon)\|_\infty \sim w_f(1/N), \quad (9)$$

with the expansion moments  $c_n$  corrected by the Jackson kernel, i.e.,

$$c_n \rightarrow \tilde{c}_n = c_n h_n. \quad (10)$$

We thus conclude that the kernel Fourier series expansion has uniform convergence with error  $O(1/N)$ . This correction applies in the same way to the expansion of the DOS and local observables.

### C. Measurement cost of the expansion moments

In the QKFE algorithm, the Fourier moments  $c_n$  are obtained from  $R$  instances of random state sampling. The number of quantum projective measurements to perform for each Fourier moment is denoted as  $K$ . We denote the noise in the single-shot measurement of  $c_n$  as  $\eta_n$ . The noise  $\eta_n$  is a random variable that fluctuates in different quantum projective measurements or for different sampled random states. Its mean is zero, and its variance is order 1, as it corresponds to the fluctuation of measuring a Pauli  $\hat{\sigma}_x$  operator [Fig. 1(a)]. The induced noise for the density of states is

$$\mathcal{E}(\epsilon) = 2 \sum_{n=1}^{N-1} \eta_n h_n \cos(n\pi\epsilon). \quad (11)$$

This represents the error of estimating the density of states based on one single projective measurement on each Fourier moment  $c_n$ . Its statistical variance is

$$\text{Var}[\mathcal{E}(\epsilon)] = 4 \sum_{n=1}^{N-1} \text{Var}(\eta_n) [h_n \cos(n\pi\epsilon)]^2. \quad (12)$$

Since both  $\text{Var}(\eta_n)$  and  $h_n$  are bounded, the variance of  $\mathcal{E}$  scales as  $\text{Var}(\mathcal{E}) \sim N$ . This scaling is independent of  $\epsilon$ , despite the  $\epsilon$  dependence of  $\mathcal{E}(\epsilon)$ . Averaging  $K$  times, the measurement precision of the density of states is then  $O(\sqrt{N/K})$  because different quantum projective measurements are completely independent of each other. Since the truncation error in the Fourier expansion is  $O(1/N)$ , as discussed above, it is reasonable to demand the same scaling for the measurement precision, which then implies a requirement for the number of repeated projective measurements

$$K \sim N^3. \quad (13)$$

In calculating other observables, the requirement for the measurement cost is the same as the density of states, according to the expansion in Eq. (5).

### D. Numerical demonstration on spin and fermion models

To benchmark the overall performance of our QKFE, we apply this algorithm to three lattice models, including a one-dimensional (1D) spin-1/2 XXZ chain,

$$\hat{H}_{1\text{D-XXZ}} = \frac{1}{2} \sum_j \hat{\sigma}_j^x \hat{\sigma}_{j+1}^x + \hat{\sigma}_j^y \hat{\sigma}_{j+1}^y + \Delta \hat{\sigma}_j^z \hat{\sigma}_{j+1}^z, \quad (14)$$

a two-dimensional (2D) XXZ model,

$$\hat{H}_{2\text{D-XXZ}} = \sum_{(i,j)} \hat{\sigma}_i^x \hat{\sigma}_j^x + \hat{\sigma}_i^y \hat{\sigma}_j^y + \Delta' \hat{\sigma}_i^z \hat{\sigma}_j^z, \quad (15)$$

and a 2D  $t$ - $V$  model of spinless fermions,

$$\hat{H}_{tV} = - \sum_{(i,j)} \hat{c}_i^\dagger \hat{c}_j + \hat{c}_j^\dagger \hat{c}_i + V \sum_{(i,j)} \hat{n}_i \hat{n}_j, \quad (16)$$

with the periodical boundary condition being adopted. The energy units were specified by introducing the Hamiltonian models. The unit of temperature is defined correspondingly since we take the Boltzmann constant as a unit. We choose  $L = 18$  for the 1D model and a  $4 \times 4$  square lattice for the 2D models. We emphasize that our QKFE algorithm is generic for performing finite temperature quantum simulations—it is not restricted to solving these three models. We deliberately choose both spin and fermion models here for benchmarking in order to confirm QKFE indeed applies generically to different quantum Hamiltonian systems.

In the numerical tests, we choose  $\Delta = -0.9$ ,  $\Delta' = -0.5$ , and  $V = 2$ . For local observables, we examine  $C_{1\text{D-XXZ}} \equiv \hat{\sigma}_1^z \hat{\sigma}_2^z$ ,  $C_{2\text{D-XXZ}} \equiv \hat{\sigma}_{11}^z \hat{\sigma}_{22}^z$ , and  $C_{tV} \equiv \hat{n}_{11} \hat{n}_{22} + \hat{n}_{11} \hat{n}_{33} + \hat{n}_{11} \hat{n}_{44}$  for the 1D-XXZ, 2D-XXZ, and  $t$ - $V$  models, respectively. We also checked other observables and found behavior similar to that presented here. The QKFE results (colored lines) are compared to the exact values (circles) in a broad temperature range in Fig. 2, with the Boltzmann constant taken as a unit. The surrounding shading represents the statistical errors evaluated with the standard bootstrap resampling approach [70]. Convergence is observed at  $R \rightarrow 20$ , and  $N \rightarrow 100$  for the 1D-XXZ and 2D  $t$ - $V$  models. For the 2D-XXZ model, a larger number,  $R = 400$ , is required. The 2D-XXZ model has  $U(1)$  symmetry and exhibits a Kosterlitz-Thouless transition and a region with a critical algebraic superfluid phase at finite temperature. For such physics, the physical observables as a function of energy density are more nonanalytic than the transverse field Ising model. Approximating more nonanalytic functions in the QKFE algorithm requires the expansion order to be larger and the Fourier moments to be more precise.

From the results shown in Fig. 2, it is apparent that the quantum algorithm performs well in the high temperature regime for all three models. In the low temperature regime, QKFE is no longer reliable, producing substantial computation errors. The large sampling error implies a large number of  $R$  are required at low temperature. The sizable discrepancy between the QKFE and exact calculation indicates a larger cutoff  $N$  is also needed to approximate the functions in Eqs. (3) and (6) at low temperature.

The inefficiency of QKFE at low temperature can be attributed to two aspects. First, the low energy states of the many-body Hamiltonian make only an exponentially small contribution to the expansion moments. Consequently, it is inevitable to sample an exponential number ( $R$ ) of random states because exponential precision would be required for the moments. Second, the DOS at low energy is exponentially smaller than that at high energy. This makes it difficult for the Fourier expansion to approximate the entire energy window. The exponential cost in the low energy regime was also observed in other finite temperature algorithms evaluating partition functions [71,72]. Nonetheless, the exponential speedup in QKFE for computing the moments compared with the classical KPM remains valid because these two aspects are also present in the classical KPM when simulating low-energy



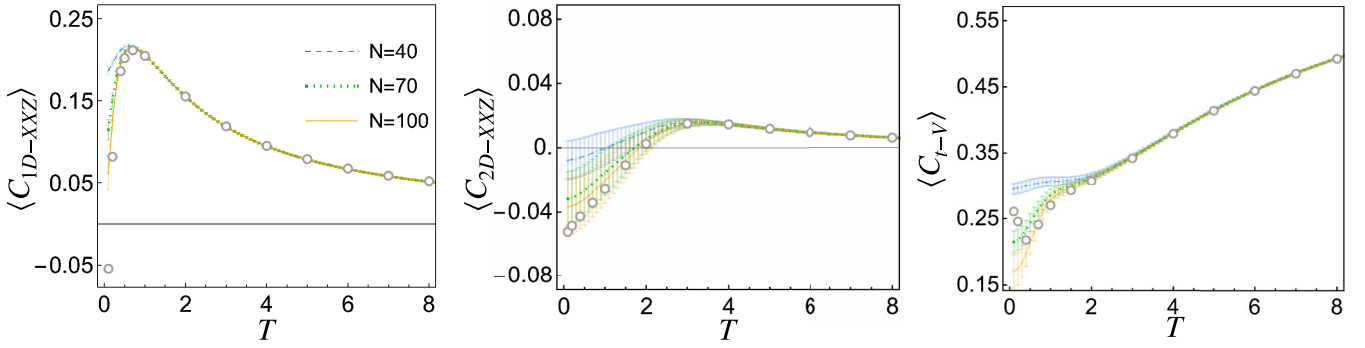


FIG. 2. Finite temperature correlations with the QKFE algorithm. The three panels from left to right correspond to the 1D-XXZ, 2D-XXZ, and  $t$ - $V$  models. For the 1D-XXZ and  $t$ - $V$  models, we choose  $R = 20$  in sampling random states, and for the 2D-XXZ model, we choose  $R = 400$ . The lines represent the numerical results using QKFE. The colored shading surrounding these lines shows sampling errors. The circles show the exact values for comparison. Here, we choose  $L = 18$  for the 1D model and a square lattice with  $4 \times 4$  geometry for the 2D models.

many-body physics. In fact, the exponential time cost for generic low temperature quantum simulations is a corollary of Hamiltonian QMA completeness [32,44,45].

### III. THERMAL ENSEMBLE ITERATION

We further develop a polynomial quantum algorithm for a restricted class of Hamiltonians assuming that its ground state determination belongs to BQP [56,73]. An efficient scheme is provided for the preparation of an excited state with finite energy density. We construct a thermal ensemble iteration protocol and show that the thermodynamic quantities, such as free energy and thermal entropy, can be obtained with polynomial cost by applying our QKFE algorithm iteratively to the finite energy quantum states. We emphasize that the thermal ensemble iteration (THEI) protocol provides a quantum algorithm for generic quantum Hamiltonian models, even for those not belonging to BQP. It is an efficient quantum algorithm for Hamiltonian models whose ground states are preparable with quantum circuits at polynomial cost.

#### A. Preparation of finite energy quantum states

For a Hamiltonian in BQP  $\hat{H}_{\text{BQP}}$ , it is guaranteed that the ground state can be reached by polynomial-depth quantum circuits that involve one- and two-qubit gates [56]. We choose a random product state to be the initial state of this quantum circuit, whose energy typically matches the infinite temperature ensemble, i.e.,  $E(\beta = 0)$ . Here,  $E(\beta)$  is the thermal ensemble average with respect to  $\hat{H}_{\text{BQP}}$ . This type of product state can be efficiently achieved due to the exponential dominance of infinite temperature states in the quantum many-body Hilbert space. The output of the quantum circuit is the ground state of  $\hat{H}_{\text{BQP}}$  with energy  $E(\beta = \infty)$ . We split the quantum circuit into multiple steps, with each step containing only one single-qubit or two-qubit gate. The gate in the  $p$ th step is denoted as  $\hat{U}_p$ , and the quantum state in this step is  $|\alpha(p)\rangle$ . The energy in the  $p$ th step is given by  $E_p = \langle \alpha(p) | \hat{H}_{\text{BQP}} | \alpha(p) \rangle$ . By physical intuition, it is reasonable to assume that the energy disturbance produced in each step, for instance,  $|E_p - E_{p-1}|$  from step  $(p-1)$  to step  $p$ , is upper bounded by a constant  $\Delta E_{\text{ub}}$  independent of the system size.

The energy density difference between two successive steps is then infinitesimal [ $O(1/L)$ ] in the thermodynamic limit. This implies that a quantum state with intermediate energy (between the ground state and infinite temperature ensemble average) can be prepared by choosing a proper intermediate  $p$  step in the polynomial-depth quantum circuit preparing the ground state. The energy density resolution of this scheme for preparing an excited state with a given energy is  $\Delta E_{\text{ub}}/L$ .

Now, we show the energy disturbance caused by one step of the quantum gate operation indeed has a rigorous upper bound for a  $k$ -local Hamiltonian. The Hamiltonian we consider has the general form  $\hat{H}_{\text{BQP}} = \sum_l \hat{H}_l$ , which acts on  $L$  qubits. Without loss of generality, we assume  $H_l$  is a Pauli operator of the form  $\hat{H}_l = J \hat{\sigma}_{i_1} \cdots \hat{\sigma}_{i_{|h_l|}}$ , with  $h_l$  representing the set of qubits that  $\hat{H}_l$  acts on. To proceed, we expand the quantum state  $|\alpha(p-1)\rangle$  at step  $(p-1)$  in the computation basis  $|\mathbf{z}\rangle$ ,  $|\alpha(p-1)\rangle = \sum_{\mathbf{z}} \psi_{\mathbf{z}} |\mathbf{z}\rangle$ . It follows that  $|\alpha(p)\rangle = \sum_{\mathbf{z}} \psi_{\mathbf{z}} |\tilde{\mathbf{z}}\rangle$ , with  $|\tilde{\mathbf{z}}\rangle \equiv \hat{U}_p |\mathbf{z}\rangle$ . Since  $\hat{U}_p$  represents a one- or two-qubit gate, the state  $|\tilde{\mathbf{z}}\rangle$  is different from  $|\mathbf{z}\rangle$  only within a local region  $g_p$ , defined to be the set of qubits that  $\hat{U}_p$  acts on. The energy difference  $\Delta E_p = E_p - E_{p-1}$  has the form

$$\Delta E_p = \sum_l \sum_{\mathbf{z}_1, \mathbf{z}_2} \psi_{\mathbf{z}_2}^* \psi_{\mathbf{z}_1} [\langle \tilde{\mathbf{z}}_2 | \hat{H}_l | \tilde{\mathbf{z}}_1 \rangle - \langle \mathbf{z}_2 | \hat{H}_l | \mathbf{z}_1 \rangle].$$

The difference in the summation is finite only when  $h_l \cap g_p \neq \emptyset$ . We then have

$$|\Delta E_p| \leq \sum_{\substack{l \\ (h_l \cap g_p \neq \emptyset)}} \sum_{\mathbf{z}_1} \sum_{\mathbf{z}_2 \in \Xi_{l, \mathbf{z}_1}} |\psi_{\mathbf{z}_2}| |\psi_{\mathbf{z}_1}| \times [|\langle \tilde{\mathbf{z}}_2 | \hat{H}_l | \tilde{\mathbf{z}}_1 \rangle - \langle \mathbf{z}_2 | \hat{H}_l | \mathbf{z}_1 \rangle|].$$

Here, the set  $\Xi_{l, \mathbf{z}_1}$  contains all  $\mathbf{z}_2$  configurations that differ from  $\mathbf{z}_1$  only in the local region  $h_l$ . In the following, the constrained summation over  $l$ ,  $\mathbf{z}_1$ , and  $\mathbf{z}_2$  as restricted by  $h_l \cap g_p \neq \emptyset$  and  $\mathbf{z}_2 \in \Xi_{l, \mathbf{z}_1}$  is denoted  $\sum'_{l, \mathbf{z}_1, \mathbf{z}_2}$  for brevity. Summing over  $l$  with the restriction  $h_l \cap g_p \neq \emptyset$  is correspondingly denoted as  $\sum'_l$ . Since the quantity in the brackets is bounded by  $|\langle \tilde{\mathbf{z}}_2 | \hat{H}_l | \tilde{\mathbf{z}}_1 \rangle - \langle \mathbf{z}_2 | \hat{H}_l | \mathbf{z}_1 \rangle| \leq 2|J|$ , we have

$$|\Delta E_p| \leq 2|J| \sum'_{l, \mathbf{z}_1, \mathbf{z}_2} |\psi_{\mathbf{z}_1}| |\psi_{\mathbf{z}_2}|.$$

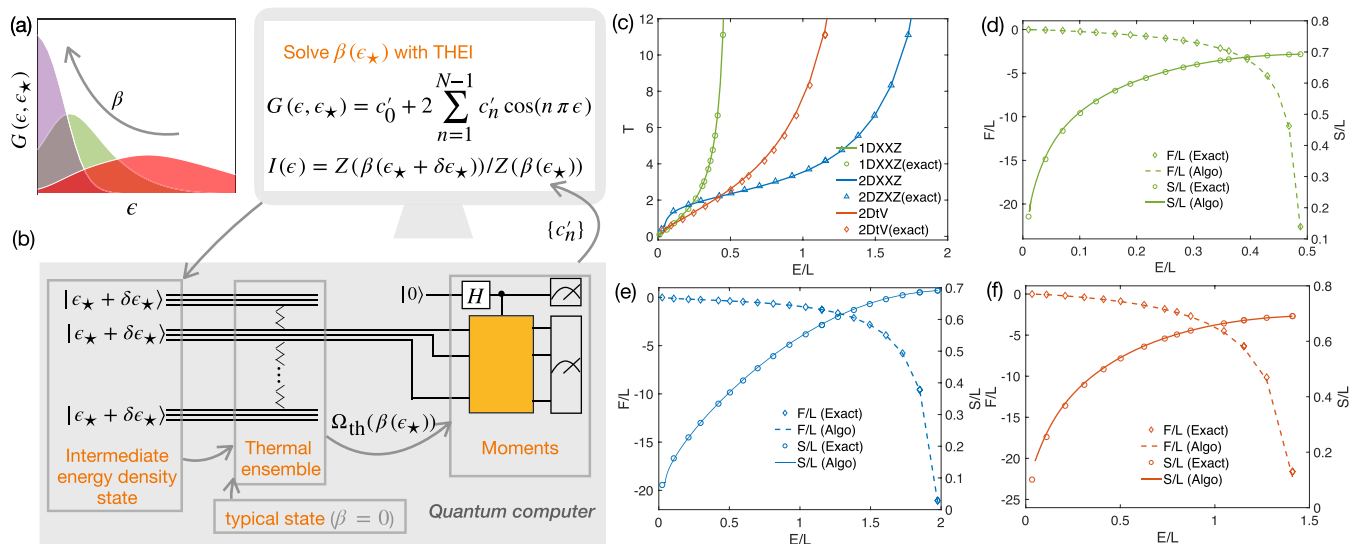


FIG. 3. Free energy and thermal entropy with the THEI protocol. (a) and (b) Schematic illustration of the THEI protocol. (c)–(f) The computed thermodynamic quantities from the THEI protocol. We study 1D-XXZ, 2D-XXZ, and 2D  $t$ -V fermion models to demonstrate the generic applicability of our quantum algorithm. (c) The energy density dependence of the inverse temperature  $\beta(E)$ . (d)–(f) The free energy and thermal entropy as a function of energy density, corresponding to the 1D-XXZ, 2D-XXZ, and  $t$ -V models, respectively. We choose  $L = 18$  for the 1D model and a square lattice with  $4 \times 4$  geometry for the 2D models. The lines represent the results of THEI, and the circles, diamonds, and triangles show the exact values for comparison. Here, we choose expansion order  $N = 100$ . The difference between the THEI and exact results is barely noticeable and can be further improved by using a larger expansion order.

Using the inequality

$$\sum_{l, z_1, z_2} |\psi_{z_1}| |\psi_{z_2}| \leq \frac{1}{2} \sum_{l, z_1, z_2} |\psi_{z_1}|^2 + |\psi_{z_2}|^2 = \sum_l 2^{|h_l|},$$

we obtain

$$|\Delta E_p| \leq \Delta E_{ub} = \gamma |J|, \quad (17)$$

with the constant  $\gamma = \sum_l 2^{|h_l|+1}$ . The energy disturbance  $\Delta E_p$  has an upper bound that is independent of the system size  $L$  for a  $k$ -local Hamiltonian.

We remark here that the above analysis applies generically for  $k$ -local Hamiltonians, including those not belonging to BQP. This means the preparation scheme described here for finite energy quantum states is applicable to all  $k$ -local Hamiltonians. Its polynomial complexity relies on assuming the ground state is preparable at polynomial cost. Our finite energy state preparation scheme implies that the finite temperature quantum simulation is, in general, at most as complicated as the ground state quantum simulation.

### B. The procedure for thermal ensemble iteration

For finite energy quantum states, although the correlation functions and local observables can be measured directly, it is still a challenge to determine the thermodynamic quantities, such as temperature, thermal entropy, and free energy. This challenge arises broadly for finite temperature quantum simulations [32,34,36]. Here, we construct a thermal ensemble iteration protocol and show that those thermodynamic quantities can be efficiently computed by an iterative running of QKFE algorithms.

Our THEI protocol is based on measuring the Fourier moments with respect to the canonical ensemble average,

$$c'_n(\epsilon_*) \equiv \text{Re}\{\text{Tr}[\hat{\Omega}_{\text{th}} e^{-in\pi \hat{\mathcal{H}}_{\text{BQP}}}\}], \quad (18)$$

which can be obtained by performing QKFE on a canonical ensemble  $\hat{\Omega}_{\text{th}} = e^{-\beta \hat{H}_{\text{BQP}}}/Z(\beta)$  (Fig. 3). Here,  $\epsilon_*$  is the ensemble average energy [rescaled according to Eq. (1)], which can be measured directly on the quantum circuit. Since the average of the unitary operator  $e^{-in\pi \hat{\mathcal{H}}_{\text{BQP}}}$  is now performed over the canonical ensemble instead of random states as in Sec. II, the Fourier moments  $c'_n$  acquire energy  $\epsilon_*$  dependence, or, equivalently,  $\beta$  dependence. There is a one-to-one correspondence between  $\epsilon_*$  and  $\beta$ . This defines the function relation  $\beta(\epsilon_*)$ , in spite of the difficulty of inferring this relation directly in the quantum circuit.

In order to prepare the canonical ensemble, we propose preparing multiple ( $M$ ) copies of  $\hat{H}_{\text{BQP}}$ , which are allowed to exchange energy only by weak interactions. Each copy is prepared in an intermediate energy density state following the protocol described in Sec. III A. It has been proved that the reduced density matrix of each copy is typically very close to the canonical ensemble, with a trace distance that decays exponentially with  $M$  [59]. According to the matrix Hölder inequality [74], the trace distance sets an upper bound for  $|c'_n - \tilde{c}'_n|$  ( $c'_n$  and  $\tilde{c}'_n$  are the Fourier moments from the exact and prepared approximate canonical ensembles, respectively). This implies the error  $|c'_n - \tilde{c}'_n|$  converges exponentially to zero with an increasing number of copies  $M$ . Alternatively, the canonical ensemble can also be prepared by considering engineering dissipation such that the steady state is a mixed state corresponding to the canonical ensemble [75].

Having the expansion moments [Eq. (18)] measured by running QKFE with the canonical ensemble as its input, the energy distribution function  $\rho(\epsilon)e^{-\beta(\epsilon_\star)\epsilon E_w}/Z(\beta)$  is then approximated by

$$G(\epsilon, \epsilon_\star) = c'_0(\epsilon_\star) + 2 \sum_{n=1}^{N-1} c'_n(\epsilon_\star) \cos(n\pi\epsilon). \quad (19)$$

It is apparent that

$$\frac{\rho(\epsilon)e^{-\beta(\epsilon_\star)\epsilon E_w}}{\rho(\epsilon)e^{-\beta(\epsilon_\star+\delta\epsilon_\star)\epsilon E_w}} \frac{e^{\beta(\epsilon_\star)\epsilon E_w}}{e^{\beta(\epsilon_\star+\delta\epsilon_\star)\epsilon E_w}}$$

is trivially independent of  $\epsilon$  by definition. This simple consideration implies a nontrivial condition on  $G(\epsilon, \epsilon_\star)$ : the function

$$I(\epsilon) \equiv \frac{G(\epsilon, \epsilon_\star)}{G(\epsilon, \epsilon_\star + \delta\epsilon_\star)} \frac{e^{\beta(\epsilon_\star)\epsilon E_w}}{e^{\beta(\epsilon_\star+\delta\epsilon_\star)\epsilon E_w}} \quad (20)$$

should be independent of  $\epsilon$ . Suppose  $\beta(\epsilon_\star)$  is already known; then the function  $I(\epsilon)$  satisfies the  $\epsilon$ -independent condition only if  $\beta(\epsilon_\star + \delta\epsilon_\star)$  is correct because otherwise, the incorrectness would produce an artificial exponential  $\epsilon$  dependence. We then determine the correct value for  $\beta(\epsilon_\star + \delta\epsilon_\star)$  by minimizing the  $\epsilon$  dependence of  $I(\epsilon)$ ,

$$\beta(\epsilon_\star + \delta\epsilon_\star) \leftarrow \min \left\{ 1 - \left[ \frac{\int d\epsilon I(\epsilon)}{\int d\epsilon I^2(\epsilon)} \right]^2 \right\}. \quad (21)$$

This defines an iteration from  $\beta(\epsilon_\star)$  to  $\beta(\epsilon_\star + \delta\epsilon_\star)$  and directly produces the ratio of the partition function,  $Z(\beta(\epsilon_\star + \delta\epsilon_\star))/Z(\beta(\epsilon_\star))$ . How close  $I(\epsilon)$  is to a constant function in the actual computation can be used as a self-verification indicator for whether the canonical ensemble has, indeed, been reached. The THEI protocol is summarized in Algorithm 1.

Since the inverse temperature  $\beta(\epsilon_\star)$  is known at the infinite temperature limit, the function  $\beta(\epsilon_\star)$  is then obtained by following the iteration from  $\epsilon_\star$  to  $\epsilon_\star + \delta\epsilon_\star$  step by step [Fig. 3(a)]. Likewise, the partition function at  $\beta = 0$  is also trivially given,  $Z(\beta = 0) = D$ . The iteration by Eq. (20) then also produces

---

Algorithm 1. Thermal ensemble iteration algorithm.

---

### Preparation

Initial product state  $|\psi_0\rangle$  with  $\langle\psi_0|\hat{H}_{\text{BQP}}|\psi_0\rangle = E(\beta = 0)$ .  
 Ground state circuit  $\mathcal{U}$  for BQP Hamiltonian.  
 $M$  copies of  $\hat{H}_{\text{BQP}}$  that can interact via  $\lambda \sum_{m=1}^{M-1} \hat{V}^{m,m+1}$ .  
 The target value of simulated inverse temperature  $\beta_{\text{tar}}$ .

### Procedure

- 1 Initialize:  $|\epsilon_\star\rangle = |\psi_0\rangle$  ( $\beta(\epsilon_\star) = 0$ ),  $\mathcal{U} = \text{Identity}$ ,  $\lambda = 0$ .
  - 2 Add single step to the circuit  $\mathcal{U} \rightarrow U_p \mathcal{U}$  and prepare  $|\epsilon_\star + \delta\epsilon_\star\rangle = \mathcal{U}|\psi_0\rangle$ .
  - 3 Turn on  $\lambda$  ( $\lambda \ll 1$ ) slowly and allow the system evolve for sufficient thermalization, then turn off  $\lambda$  slowly.
  - 4 Perform the QKFE algorithm for each copy to get  $c'_n$ , then construct  $G(\epsilon, \epsilon_\star)$  as Eq. (19) and  $I(\epsilon)$  as Eq. (20).
  - 5 Solve  $\beta(\epsilon_\star + \delta\epsilon_\star)$  with Eq. (21).
  - 6 If  $\beta(\epsilon_\star + \delta\epsilon_\star) > \beta_{\text{tar}}$ , reset  $\epsilon_\star \rightarrow \epsilon_\star + \delta\epsilon_\star$ ,  $\beta(\epsilon_\star) \rightarrow \beta(\epsilon_\star + \delta\epsilon_\star)$ , then go back to 2. Else, stop.
- 

the partition function  $Z(\beta)$ , from which the free energy is given by  $F(\beta) = -\log Z(\beta)/\beta$ , and the thermal entropy is given by  $S(\beta) = \beta[E(\beta) - F(\beta)]$  with the Boltzmann constant taken as a unit.

### C. Stepping complexity of the THEI protocol

In our THEI protocol, the thermodynamic properties of a canonical ensemble are obtained by stepping from the infinite temperature limit to a finite temperature. Here, we analyze the stepping complexity of the THEI protocol. From the uniform convergence of the kernel Fourier expansion, the energy distribution function  $\rho(\epsilon)e^{-\beta\epsilon E_w}/Z(\beta)$  is well approximated by the expansion  $G(\epsilon, \epsilon_\star)$  in the energy window  $[\epsilon_\star - \sigma_\epsilon, \epsilon_\star + \sigma_\epsilon]$ , with  $\sigma_\epsilon$  characterizing the energy fluctuation of the canonical ensemble (rescaled by  $E_w$  in our notation) that scales with the system size as  $1/\sqrt{L}$  [66]. Within this window both the absolute and relative errors are suppressed by  $O(1/N)$  (see Sec. II B), whereas outside this energy window, the expanded function can be exponentially small, and the relative error is no longer controllable. This sets a requirement for the stepping in the THEI protocol: the step in  $\epsilon_\star$ ,  $\delta\epsilon_\star$ , should scale with  $\sigma_\epsilon$ , i.e.,

$$\delta\epsilon_\star \sim 1/\sqrt{L}. \quad (22)$$

Computing a thermodynamic quantity as a function of  $\beta$  using THEI then involves  $O(\sqrt{L})$  runs of QKFE.

In the THEI protocol, the finite energy states have to be prepared following the scheme in Sec. III A repeatedly. The number of repeats scales polynomially as  $O(N^4\sqrt{L})$ , with the measurement cost taken into account (Sec. II C). In order to reduce the quantum state preparation cost, it is worth considering further integrating a quantum nondemolition measurement [76] to our scheme to determine the expansion moments of Eq. (18), which is expected to improve the efficiency of our THEI protocol. This is left for future investigation.

### D. Numerical demonstration

We apply the THEI protocol to the 1D-XXZ, 2D-XXZ, and  $t$ - $V$  models, which were introduced in Sec. II D, and examine its performance from high to low temperatures. The results are shown in Fig. 3. We confirm the computed inverse temperature, free energy, and thermal entropy by the iteration protocol matches to the exact values, with errors being barely noticeable. It is evident this protocol performs well for the entire temperature range for all three models. The large discrepancy observed for the original QKFE in Fig. 2 at low temperature is no longer present with the THEI protocol [Figs. 3(c)–3(f)]. With our numerical demonstration using one fermion and two spin models, we believe that the THEI protocol with a polynomial cost for a quantum device is generically applicable to finite temperature quantum simulations of quantum Hamiltonian models.

## IV. EXPERIMENTAL REALIZATION

One key building block for our quantum algorithms including QKFE and THEI is the control unitary shown in Fig. 1. In this section we discuss its physical realization, considering

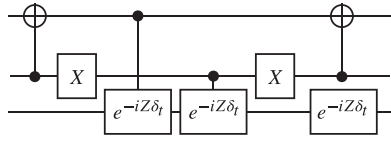


FIG. 4. Quantum circuit diagram decomposition of the controlled-ZZ evolution with one- and two-qubit gates.

both a digital quantum circuit and analog quantum simulation devices, and analyze the actual implementation cost.

### A. Realization with digital quantum circuits

To realize of our quantum algorithms using digital quantum computation, we consider Trotterizing the control unitary in Eq. (4). One Trotter step is  $|0\rangle\langle 0| \otimes I + |1\rangle\langle 1| \otimes e^{-i\hat{H}\delta_t}$ , with  $\delta_t$  controlling the Trotter error. To be concrete, we consider spin models containing one- and two-body interactions. The control unitary corresponding to the one-body terms is realized by a control-phase gate [77]. The control unitary corresponding to the two-body terms can be constructed with three-qubit gates like C-ISWAP gates or Toffoli gates, as proposed in Ref. [78]. In Fig. 4 we provide an efficient gate decomposition using only one- and two-qubit gates for a control unitary corresponding to the two-body terms, the controlled-ZZ evolution. The controlled-XX or -YY evolution can be decomposed in a similar way with four additional single-qubit rotation operations. Taking the 1D-XXZ spin chain as one example, the Trotter realization of the control unitary in Eq. (4) involves  $15(L-1)n\pi\delta_t^{-1}$  two-qubit gates. The depth of the QKFE circuit then scales as  $O(\delta_t^{-1}N)$ . The required number of two-qubit gates will determine the size of the quantum simulation problem that can be performed on near-term quantum devices. With the scheme provided here, performing QKFE on the 1D-XXZ spin chain with  $L=4$ ,  $N=3$ , and  $\delta_t=0.2\pi$  would require a total of 675 two-qubit gates. At the same time, we believe that the quantum circuit realization can be further simplified with recently developed circuit-depth reduction techniques [79–81], which is left for future investigation. An experimental demonstration of QKFE is within reasonable accessibility of superconducting qubit systems. For the linear scaling of the QKFE circuit depth in  $\delta_t^{-1}$  and  $N$ , we anticipate that a finite temperature quantum simulation based on our proposed quantum algorithms could reach beyond classical simulation capability with near-term quantum technology.

### B. Realization with an atom-based analog quantum simulator

Here, we take the 1D-XXZ model as an example and provide an experimental realization of the control unitary in Eq. (4) with an atom-based quantum simulation system. We consider a system of ultracold atoms confined in a periodic optical lattice. The atoms are prepared in two hyperfine states with the Zeeman sublevels representing two spin-1/2 states. In the Mott insulator regime, the system is described by an effective XXZ Hamiltonian [82],

$$\hat{H} = \sum_{\langle ij \rangle} [J_{xy}(\sigma_i^x \sigma_j^x + \sigma_i^y \sigma_j^y) + J_z \sigma_i^z \sigma_j^z], \quad (23)$$

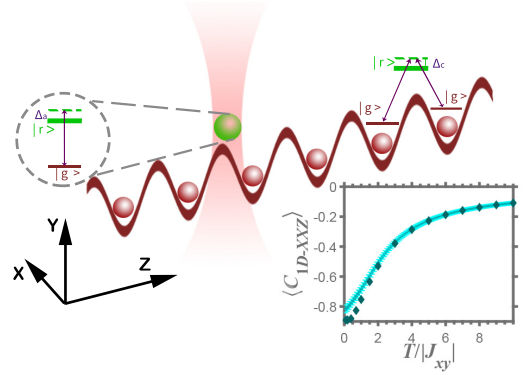


FIG. 5. Experiment protocol for implementing the QKFE algorithm on an analog quantum simulator based on atoms confined in an optical lattice and optical tweezers. This setup implements the QKFE algorithm for the 1D-XXZ model (see the text). Finite temperature correlations of the 1D-XXZ model  $C_{1D-XXZ} = \langle \hat{\sigma}_1^z \hat{\sigma}_2^z \rangle$  with QKFE (blue line) are shown in the inset and compared to the exact results (diamonds). The results are calculated with  $N=14$  and  $R=100$  using the parameters of the proposed Rydberg atom experiment in Sec. IV B.

where the spin coupling is mediated by superexchange. We have  $J_{xy} = -t^2/U_{\uparrow\downarrow}$  and  $J_z = t^2/U_{\uparrow\downarrow} - (t^2/U_{\uparrow\uparrow} + t^2/U_{\downarrow\downarrow})$ , with  $t$  being the single-particle tunneling across nearby lattice sites and  $U_{\sigma\sigma'}$  being the on-site Hubbard interactions. In this system, the anisotropy  $\Delta = J_z/J_{xy}$  is tunable through the Feshbach resonance.

We introduce a separately controllable atom as the ancilla qubit confined with optical tweezers in Fig. 5. The ancilla qubit can be encoded by two hyperfine ground states dressed with Rydberg excitations. The control unitary corresponding to the Hamiltonian in Eq. (23) is then realized by combining Raman-induced tunneling [83,84] and Rydberg blockade [76,85]. The direct atomic tunnelings should be suppressed by adding a large enough linear tilt potential to the optical lattice. The Raman-assisted coupling between neighboring sites is then enabled by setting the Raman detuning  $\delta$  resonant with the energy offset of the nearby lattice sites. By using a Rydberg state as the intermediate state of the Raman transition, the Raman-assisted tunneling can then be switched on and off according to the ancilla qubit.

To be more concrete, we consider  $^{87}\text{Rb}$  atoms as carriers of both the control unitary and ancilla qubits. The lattice depth is set as  $V_x, V_y = 30E_R$  ( $E_R$  is the recoil energy) in the  $x$  and  $y$  directions and  $V_z = 3.6E_R$  in the  $z$  direction tilted by a spin-independent linear potential  $\Delta_L = h \times 2.0$  kHz per site, with  $h$  being the Planck constant. This setup leads to a 1D tilted lattice, as shown in Fig. 5. The Raman process is established via single-photon coupling to the Rydberg state as the intermediate state [86], with a single-photon Rabi frequency  $\Omega_c = 17$  kHz and single-photon detuning  $\Delta_c = 300$  kHz. This set of optimized parameters lies in the Mott insulator regime and leads to isotropic superexchange interactions  $J_{xy} = J_z = -h \times 2.78$  Hz in the absence of Feshbach resonance. For the ancilla qubit encoding, we use the Raman laser to selectively dress one of the two encoding hyperfine ground states. The fraction of Rydberg excitations in the dressing scheme is maintained at a certain level for a sufficiently long lifetime.



Here, we assume the ancilla qubit is placed properly such that the bare Rydberg interaction energy  $\Delta_{r-r}$  between lattice confined atoms and the ancilla qubit satisfies  $\Delta_{r-r} \geq 1$  GHz [87]. Then the ancilla qubit in the Rydberg dressed state will cause an energy shift  $\Delta_{r-r}\Omega_a^2/(4\Delta_a^2) \geq 800$  kHz on the Raman intermediate state of each atom in the 1D lattice, which consequently switches off the Raman-assisted tunneling. The Raman-assisted tunneling is on for the ancilla in the other encoding hyperfine state.

We choose Rydberg state  $110P$  with an estimated lifetime  $\tau_0 \approx 1.7$  ms [88,89] for both the Raman intermediate state and ancilla Rydberg dressing. The lifetime of the composite system of  $L = 6$  lattice qubits and the ancilla is above 300 ms with our Rydberg dressing scheme. Suppose that the experimental system is allowed to run for 170 ms, i.e., within its lifetime, the QKFE algorithm can be performed to  $N = 14$  orders for the XXZ model in Eq. (23) with the above superexchange interaction. With this setup, we calculate the finite temperature correlation  $\hat{\sigma}_i^z \hat{\sigma}_j^z$  using QKFE by averaging  $R = 100$  random states and show the results in the inset of Fig. 5. The QKFE results agree well with the exact results, having a tiny discrepancy only in the low temperature regime with  $T/|J_{xy}| < 1$ .

We remark here that the control unitary for the 2D XXZ model can be realized in a similar way using a 2D square lattice, where the linear tilt potential should be added along the diagonal direction of the lattice. The ancilla qubit can be placed near the lattice plane. In addition, the experimental proposal can be made even more efficient with  $^{39}\text{K}$  atoms [90] since the superexchange is naturally stronger for lighter atoms. In the meantime, the coupling strengths have a much larger degree of tunability using Feshbach resonances of  $^{39}\text{K}$  [91].

## V. CONCLUSION

We proposed a quantum kernel function expansion algorithm for finite temperature quantum simulations, where the

key is to expand the density of states and energy dependence of local observables by a Jackson kernel corrected Fourier series. The QKFE algorithm completely lacks variational optimization, which is required in other quantum Hamiltonian algorithms such as variational quantum eigensolvers and quantum Lanczos methods. For a generic Hamiltonian, the QKFE algorithm has an exponential quantum advantage compared to its classical analog, namely, the classical KPM, in computing expansion moments. For a BQP Hamiltonian, we equipped QKFE with a THEI protocol, which constitutes an efficient finite temperature quantum simulation method for computing thermodynamic quantities such as free energy and thermal entropy with a polynomial time cost. For a more general Hamiltonian beyond BQP, the THEI protocol remains applicable, and its time cost for performing finite temperature quantum simulations is comparable to finding the ground state of the Hamiltonian. In analyzing the experimental realization considering superconducting qubit and Rydberg atom quantum simulating platforms, we found the QKFE algorithm is accessible to current quantum technology. Whether the quantum advantage persists in the presence of experimental noise is related to a broader open question of establishing the quantum advantage of noisy intermediate-scale quantum devices [92–95], which is left for future investigation.

## ACKNOWLEDGMENTS

We acknowledge helpful discussions with P. Zoller, D. Vasilyev, and L. Kharkwal Joshi. This work is supported by the National Program on Key Basic Research Project of China (Grant No. 2021YFA1400900), the National Natural Science Foundation of China (Grants No. 11934002 and No. 92165203), the Shanghai Municipal Science and Technology Major Project (Grant No. 2019SHZDZX01), and the Shanghai Science Foundation (Grant No. 21QA1400500).

- 
- [1] B. Bauer, S. Bravyi, M. Motta, and G. K.-L. Chan, *Chem. Rev.* **120**, 12685 (2020).
  - [2] S. McArdle, S. Endo, A. Aspuru-Guzik, S. C. Benjamin, and X. Yuan, *Rev. Mod. Phys.* **92**, 015003 (2020).
  - [3] P. A. M. Dirac, *Proc. R. Soc. London, Ser. A* **123**, 714 (1929).
  - [4] R. P. Feynman, *Int. J. Theor. Phys.* **21**, 467 (1982).
  - [5] S. Sachdev, *Nat. Phys.* **4**, 173 (2008).
  - [6] B. Keimer, S. A. Kivelson, M. R. Norman, S. Uchida, and J. Zaanen, *Nature (London)* **518**, 179 (2015).
  - [7] A. Mann, *Nature (London)* **579**, 20 (2020).
  - [8] J. I. Cirac and P. Zoller, *Phys. Today* **57**(3), 38 (2004).
  - [9] S. Giorgini, L. P. Pitaevskii, and S. Stringari, *Rev. Mod. Phys.* **80**, 1215 (2008).
  - [10] I. M. Georgescu, S. Ashhab, and F. Nori, *Rev. Mod. Phys.* **86**, 153 (2014).
  - [11] M. P. A. Fisher, P. B. Weichman, G. Grinstein, and D. S. Fisher, *Phys. Rev. B* **40**, 546 (1989).
  - [12] M. Greiner, O. Mandel, T. Esslinger, T. W. Hänsch, and I. Bloch, *Nature (London)* **415**, 39 (2002).
  - [13] C. A. Regal, M. Greiner, and D. S. Jin, *Phys. Rev. Lett.* **92**, 040403 (2004).
  - [14] R. A. Hart, P. M. Duarte, T.-L. Yang, X. Liu, T. Paiva, E. Khatami, R. T. Scalettar, N. Trivedi, D. A. Huse, and R. G. Hulet, *Nature (London)* **519**, 211 (2015).
  - [15] T. A. Hilker, G. Salomon, F. Grusdt, A. Omran, M. Boll, E. Demler, I. Bloch, and C. Gross, *Science* **357**, 484 (2017).
  - [16] A. Mazurenko, C. S. Chiu, G. Ji, M. F. Parsons, M. Kanász-Nagy, R. Schmidt, F. Grusdt, E. Demler, D. Greif, and M. Greiner, *Nature (London)* **545**, 462 (2017).
  - [17] F. Arute *et al.*, *Nature (London)* **574**, 505 (2019).
  - [18] K. Satzinger *et al.*, *Science* **374**, 1237 (2021).
  - [19] M. Gong *et al.*, *Science* **372**, 948 (2021).
  - [20] Y. Wu *et al.*, *Phys. Rev. Lett.* **127**, 180501 (2021).
  - [21] J. Zhang, G. Pagano, P. W. Hess, A. Kyprianidis, P. Becker, H. Kaplan, A. V. Gorshkov, Z. X. Gong, and C. Monroe, *Nature (London)* **551**, 601 (2017).

- [22] C. Kokail, C. Maier, R. van Bijnen, T. Brydges, M. K. Joshi, P. Jurcevic, C. A. Muschik, P. Silvi, R. Blatt, C. F. Roos, and P. Zoller, *Nature (London)* **569**, 355 (2019).
- [23] M. Tillmann, B. Dakić, R. Heilmann, S. Nolte, A. Szameit, and P. Walther, *Nat. Photonics* **7**, 540 (2013).
- [24] A. Crespi, R. Osellame, R. Ramponi, D. J. Brod, E. F. Galvão, N. Spagnolo, C. Vitelli, E. Maiorino, P. Mataloni, and F. Sciarrino, *Nat. Photonics* **7**, 545 (2013).
- [25] M. A. Broome, A. Fedrizzi, S. Rahimi-Keshari, J. Dove, S. Aaronson, T. C. Ralph, and A. G. White, *Science* **339**, 794 (2013).
- [26] J. B. Spring, B. J. Metcalf, P. C. Humphreys, W. S. Kolthammer, X.-M. Jin, M. Barbieri, A. Datta, N. Thomas-Peter, N. K. Langford, D. Kundys *et al.*, *Science* **339**, 798 (2013).
- [27] H.-S. Zhong *et al.*, *Science* **370**, 1460 (2020).
- [28] H. Labuhn, D. Barredo, S. Ravets, S. de Léséleuc, T. Macrì, T. Lahaye, and A. Browaeys, *Nature (London)* **534**, 667 (2016).
- [29] H. Bernien, S. Schwartz, A. Keesling, H. Levine, A. Omran, H. Pichler, S. Choi, A. S. Zibrov, M. Endres, M. Greiner, V. Vuletić, and M. D. Lukin, *Nature (London)* **551**, 579 (2017).
- [30] S. de Léséleuc, V. Lienhard, P. Scholl, D. Barredo, S. Weber, N. Lang, H. P. Büchler, T. Lahaye, and A. Browaeys, *Science* **365**, 775 (2019).
- [31] G. Semeghini, H. Levine, A. Keesling, S. Ebadi, T. T. Wang, D. Bluvstein, R. Verresen, H. Pichler, M. Kalinowski, R. Samajdar *et al.*, *Science* **374**, 1242 (2021).
- [32] K. Temme, T. J. Osborne, K. G. Vollbrecht, D. Poulin, and F. Verstraete, *Nature (London)* **471**, 87 (2011).
- [33] M.-H. Yung and A. Aspuru-Guzik, *Proc. Natl. Acad. Sci. USA* **109**, 754 (2012).
- [34] M. Motta, C. Sun, A. T. K. Tan, M. J. O'Rourke, E. Ye, A. J. Minnich, F. G. S. L. Brandão, and G. K.-L. Chan, *Nat. Phys.* **16**, 205 (2020).
- [35] J. Cohn, F. Yang, K. Najafi, B. Jones, and J. K. Freericks, *Phys. Rev. A* **102**, 022622 (2020).
- [36] S. Lu, M. C. Bañuls, and J. I. Cirac, *PRX Quantum* **2**, 020321 (2021).
- [37] R. Movassagh and O. Shtanko, [arXiv:2112.14688](https://arxiv.org/abs/2112.14688).
- [38] A. Aspuru-Guzik, A. D. Dutoi, P. J. Love, and M. Head-Gordon, *Science* **309**, 1704 (2005).
- [39] Y. Ge, J. Tura, and J. I. Cirac, *J. Math. Phys.* **60**, 022202 (2019).
- [40] E. Farhi, J. Goldstone, S. Gutmann, J. Lapan, A. Lundgren, and D. Preda, *Science* **292**, 472 (2001).
- [41] D. Aharonov, W. Van Dam, J. Kempe, Z. Landau, S. Lloyd, and O. Regev, *SIAM Rev.* **50**, 755 (2008).
- [42] A. Peruzzo, J. McClean, P. Shadbolt, M.-H. Yung, X.-Q. Zhou, P. J. Love, A. Aspuru-Guzik, and J. L. O'Brien, *Nat. Commun.* **5**, 4213 (2014).
- [43] M. Cerezo, A. Arrasmith, R. Babbush, S. C. Benjamin, S. Endo, K. Fujii, J. R. McClean, K. Mitarai, X. Yuan, L. Cincio, and P. J. Coles, *Nat. Rev. Phys.* **3**, 625 (2021).
- [44] D. Poulin and P. Wocjan, *Phys. Rev. Lett.* **103**, 220502 (2009).
- [45] A. N. Chowdhury and R. D. Somma, *Quantum Inf. Comput.* **17**, 41 (2017).
- [46] J. Wu and T. H. Hsieh, *Phys. Rev. Lett.* **123**, 220502 (2019).
- [47] G. Verdon, J. Marks, S. Nanda, S. Leichenauer, and J. Hidary, [arXiv:1910.02071](https://arxiv.org/abs/1910.02071) [quant-ph].
- [48] D. Zhu, S. Johri, N. M. Linke, K. A. Landsman, C. H. Alderete, N. H. Nguyen, A. Y. Matsuura, T. H. Hsieh, and C. Monroe, *Proc. Natl. Acad. Sci. USA* **117**, 25402 (2020).
- [49] A. Weiße, G. Wellein, A. Alvermann, and H. Fehske, *Rev. Mod. Phys.* **78**, 275 (2006).
- [50] S. McArdle, T. Jones, S. Endo, Y. Li, S. C. Benjamin, and X. Yuan, *npj Quantum Inf.* **5**, 75 (2019).
- [51] K. Yeter-Aydeniz, R. C. Pooser, and G. Siopsis, *npj Quantum Inf.* **6**, 63 (2020).
- [52] C. Cao, Z. An, S.-Y. Hou, D. L. Zhou, and B. Zeng, *Commun. Phys.* **5**, 57 (2022).
- [53] J. R. McClean, S. Boixo, V. N. Smelyanskiy, R. Babbush, and H. Neven, *Nat. Commun.* **9**, 4812 (2018).
- [54] C. Ortiz Marrero, M. Kieferová, and N. Wiebe, *PRX Quantum* **2**, 040316 (2021).
- [55] J. Kempe, A. Kitaev, and O. Regev, *SIAM J. Comput.* **35**, 1070 (2006).
- [56] T. S. Cubitt and A. Montanaro, *SIAM J. Comput.* **45**, 268 (2016).
- [57] S. Gharibian, Y. Huang, Z. Landau, and S. W. Shin, *Found. Trends Theor. Comput. Sci.* **10**, 159 (2015).
- [58] J. Richter and A. Pal, *Phys. Rev. Lett.* **126**, 230501 (2021).
- [59] S. Popescu, A. J. Short, and A. Winter, *Nat. Phys.* **2**, 754 (2006).
- [60] S. Goldstein, J. L. Lebowitz, R. Tumulka, and N. Zanghì, *Phys. Rev. Lett.* **96**, 050403 (2006).
- [61] C. Bartsch and J. Gemmer, *Phys. Rev. Lett.* **102**, 110403 (2009).
- [62] S. Boixo, S. V. Isakov, V. N. Smelyanskiy, R. Babbush, N. Ding, Z. Jiang, M. Bremner, J. M. Martinis, and H. Neven, *Nat. Phys.* **14**, 595 (2018).
- [63] J. Emerson, Y. S. Weinstein, M. Saraceno, S. Lloyd, and D. G. Cory, *Science* **302**, 2098 (2003).
- [64] R. Oliveira, O. C. O. Dahlsten, and M. B. Plenio, *Phys. Rev. Lett.* **98**, 130502 (2007).
- [65] L. K. Joshi, A. Elben, A. Vikram, B. Vermersch, V. Galitski, and P. Zoller, *Phys. Rev. X* **12**, 011018 (2022).
- [66] R. K. Pathria and P. D. Beale, *Statistical Mechanics* (Elsevier, Amsterdam, 2011).
- [67] T. Morimae, K. Fujii, and J. F. Fitzsimons, *Phys. Rev. Lett.* **112**, 130502 (2014).
- [68] K. Fujii, H. Kobayashi, T. Morimae, H. Nishimura, S. Tamate, and S. Tani, *Phys. Rev. Lett.* **120**, 200502 (2018).
- [69] D. Jackson, *Trans. Am. Math. Soc.* **13**, 491 (1912).
- [70] B. Efron, *SIAM Rev.* **21**, 460 (1979).
- [71] P. Rall, *Phys. Rev. A* **102**, 022408 (2020).
- [72] A. N. Chowdhury, R. D. Somma, and Y. Subaşı, *Phys. Rev. A* **103**, 032422 (2021).
- [73] M. Nielsen and I. Chuang, *Quantum Computation and Quantum Information* (Cambridge University Press, Cambridge, 2000).
- [74] M. B. Ruskai, *Commun. Math. Phys.* **26**, 280 (1972).
- [75] S. Lieu, Y.-J. Liu, and A. V. Gorshkov, [arXiv:2205.09767](https://arxiv.org/abs/2205.09767).
- [76] D. V. Vasilyev, A. Grankin, M. A. Baranov, L. M. Sieberer, and P. Zoller, *PRX Quantum* **1**, 020302 (2020).
- [77] X. Mi *et al.*, *Nature (London)* **601**, 531 (2022).
- [78] P. Zhao, P. Xu, D. Lan, X. Tan, H. Yu, and Y. Yu, *Phys. Rev. Appl.* **14**, 064016 (2020).
- [79] Y.-H. Zhang, P.-L. Zheng, Y. Zhang, and D.-L. Deng, *Phys. Rev. Lett.* **125**, 170501 (2020).
- [80] L. Gyongyosi and S. Imre, *Sci. Rep.* **10**, 11229 (2020).
- [81] T. Fösel, M. Y. Niu, F. Marquardt, and L. Li, [arXiv:2103.07585](https://arxiv.org/abs/2103.07585).
- [82] P. N. Jepsen, J. Amato-Grill, I. Dimitrova, W. W. Ho, E. Demler, and W. Ketterle, *Nature (London)* **588**, 403 (2020).

- [83] H. Miyake, G. A. Siviloglou, C. J. Kennedy, W. C. Burton, and W. Ketterle, *Phys. Rev. Lett.* **111**, 185302 (2013).
- [84] M. Aidelsburger, M. Atala, M. Lohse, J. T. Barreiro, B. Paredes, and I. Bloch, *Phys. Rev. Lett.* **111**, 185301 (2013).
- [85] M. Saffman, T. G. Walker, and K. Mølmer, *Rev. Mod. Phys.* **82**, 2313 (2010).
- [86] S. Hollerith, J. Zeiher, J. Rui, A. Rubio-Abadal, V. Walther, T. Pohl, D. M. Stamper-Kurn, I. Bloch, and C. Gross, *Science* **364**, 664 (2019).
- [87] K. Singer, J. Stanojevic, M. Weidemüller, and R. Côté, *J. Phys. B* **38**, S295 (2005).
- [88] I. I. Beterov, I. I. Ryabtsev, D. B. Tretyakov, and V. M. Entin, *Phys. Rev. A* **79**, 052504 (2009).
- [89] J. B. Balewski, A. T. Krupp, A. Gaj, D. Peter, H. P. Büchler, R. Löw, S. Hofferberth, and T. Pfau, *Nature (London)* **502**, 664 (2013).
- [90] N. Lorenz, L. Festa, L.-M. Steinert, and C. Gross, *SciPost Phys.* **10**, 052 (2021).
- [91] C. D’Errico, M. Zaccanti, M. Fattori, G. Roati, M. Inguscio, G. Modugno, and A. Simoni, *New J. Phys.* **9**, 223 (2007).
- [92] J. Preskill, *Quantum* **2**, 79 (2018).
- [93] S. Bravyi, D. Gosset, R. Koenig, and M. Tomamichel, *Nat. Phys.* **16**, 1040 (2020).
- [94] K. Noh, L. Jiang, and B. Fefferman, *Quantum* **4**, 318 (2020).
- [95] D. Aharonov, X. Gao, Z. Landau, Y. Liu, and U. Vazirani, in *Proceedings of the 55th Annual ACM Symposium on Theory of Computing* (ACM, New York, 2023), pp. 945–957.